Origins of photoluminescence instabilities at halide perovskite/organic hole transport layer interfaces

Zhaojian Xu,[1] *Daniel D. Astridge*,[2] *Ross A. Kerner*,[3] *Xinjue Zhong*,[1] *Junnan Hu*,[1] *Jisu Hong*,[1] *Jesse A. Wisch*,[1] *Kai Zhu*,[3] *Joseph J. Berry*,[3, 4, 5] *Antoine Kahn*,[1] *Alan Sellinger*,[2, 3] *and Barry P. Rand*[1, 6*]

[1]Department of Electrical and Computer Engineering, Princeton University, Princeton, NJ 08544, USA

[2]Department of Chemistry, Colorado School of Mines, Golden, CO 80401, USA

[3]National Renewable Energy Laboratory, Golden, CO 80401, USA

[4]Renewable and Sustainable Energy Institute, University of Colorado Boulder, Boulder, CO 80309, USA

[5]Department of Physics, University of Colorado Boulder, Boulder, CO 80309, USA

[6]Andlinger Center for Energy and the Environment, Princeton University, Princeton, NJ 08544, USA

[*]Correspondence: brand@princeton.edu (B.P.R.)

Abstract

Metal halide perovskites are promising for optoelectronic device applications; however, their poor stability under solar illumination remains a primary concern. While the intrinsic photostability of isolated neat perovskite samples has been widely discussed, it is important to explore how charge transport layers – employed in most devices – impact photostability. Herein, we study the effect of organic hole transport layers (HTLs) on light-induced halide segregation and photoluminescence (PL) quenching at perovskite/organic HTL interfaces. By employing a series of organic HTLs, we demonstrate that the HTL highest occupied molecular orbital energy dictates behavior; furthermore, we reveal the key role of halogen loss from the perovskite and subsequent permeation into organic HTLs, where it acts as a PL quencher at the interface and introduces additional mass transport pathways to facilitate halide phase separation. In doing so, we both reveal the microscopic mechanism of non-radiative recombination at perovskite/organic HTL interfaces and detail the chemical rationale for closely matching the perovskite/organic HTL energetics to maximize solar cell efficiency and stability.

Introduction

Metal halide perovskites, owing to unique optoelectronic properties,[1, 2] are promising in various optoelectronic devices,[3-5] notably photovoltaics.[6-8] However, one challenge for application is relatively poor stability under external stressors, such as moisture, heat, and solar illumination.[9-12] Although some atmospheric stressors (e.g. moisture and oxygen) can be minimized through encapsulation,[13-15] light is required for solar cell operation. Thus, understanding light-induced instabilities is critical for the commercialization of perovskite photovoltaics.

Photoluminescence (PL) spectroscopy is sensitive to compositional change and carrier dynamics within the perovskite medium and can be performed *in situ*.[16] Light-induced halide segregation in mixed halide perovskites is often identified via PL, where it primarily manifests as a spectral shift. This indicates an effective bandgap instability which greatly restricts practical applications.[17] Although such a phenomenon has been heavily investigated,[17-19] most previous studies focused on isolated neat perovskite samples.[20-30] However, in a perovskite device, the perovskite layer is always in contact with charge transport layers (CTLs); thus, it is important to investigate light-induced halide segregation in the presence of CTLs to understand how they influence light-induced halide segregation.[31] In our previous work, we studied voltage-induced halide segregation probed by PL peak shifts and cross-sectional scanning transmission electron microscopy–energy dispersive X-ray spectroscopy (STEM-EDX). We found that iodine photo-electrochemistry and iodine transport pathways play important roles in halide segregation for mixed iodide/bromide perovskites, with an organic hole transport layer (HTL) providing a fast external iodine transport pathway, which depends strongly on ionization energy (IE).[32-34] Since HTLs with different highest occupied molecular orbital (HOMO) levels show drastically different iodine diffusion rates,[34] it is expected that different HTLs may have different effects on light-induced halide segregation. Therefore, an in-depth study on how different HTLs affect light-induced halide segregation is necessary for the design of stable mixed-halide perovskite-based optoelectronic devices. So far, only a few reports have looked into the effect of HTLs on light-induced halide segregation;[35-39] some observe that an HTL can accelerate light-induced halide segregation,[35, 36] while others report an opposite trend.[37-39]

Notably, only a single HTL material was used in each of those studies, making unambiguous conclusions challenging.

In addition to the PL peak shift observed for mixed-halide perovskites, another potential instability in the PL for both mixed-halide and pure-halide perovskite compositions is an intensity drop over time, i.e., light-induced PL quenching (LIPQ) or photodarkening, with increased non-radiative recombination. Additionally, PL can be enhanced [termed light-induced PL enhancement (LIPE) or photobrightening] in certain regions of the perovskite due to various effects including carrier funneling to low bandgap domains.[17, 40-42] Although many studies have discussed steady-state PL quenching at perovskite/HTL interfaces[43] and have commonly attributed it to charge extraction,[44-47] the change of PL intensity (or quantum yield) over time at perovskite/organic HTL interfaces is less discussed but highly relevant to the performance and stability under constant illumination. Further, these studies all assume ion accumulation (i.e. that the perovskite/HTL is ion blocking), but overlook the fact that halides readily permeate into the HTL bulk.[34]

In this study, we systematically investigate reactions between iodine and organic HTLs, and the effect of the organic HTL HOMO energy on the stability of the perovskite PL spectrum. The HOMO energy is defined in this work with respect to the vacuum level and is the negative of IE of the organic film. We observe non-monotonic trends in the magnitude and direction of the illumination-induced PL peak shift, PL intensity (LIPQ or LIPE), and halide diffusion into the HTL as measured by cross-sectional STEM-EDX versus organic HTL HOMO energy. These behaviors are rationalized by HOMO-dependent reactions with iodine lost from the perovskite layer and chemical speciation within the organic HTL. Thus, we conclude that the HTL HOMO energy is the key factor that ultimately determines the PL behavior at perovskite/organic HTL interfaces under illumination, where instabilities in the PL spectra are related to halogen loss from the perovskite layer into the HTL for shallow-HOMO HTLs (IE < 5.0 eV), chemical equilibrium between iodic species in the perovskite and HTL for intermediate-HOMO HTLs (IE ~ 5.2 eV), and halogen-related defects confined within the perovskite layer for deep-HOMO HTLs (IE > 5.6 eV).

Results and Discussion

Transport and interaction of iodine in organic HTLs

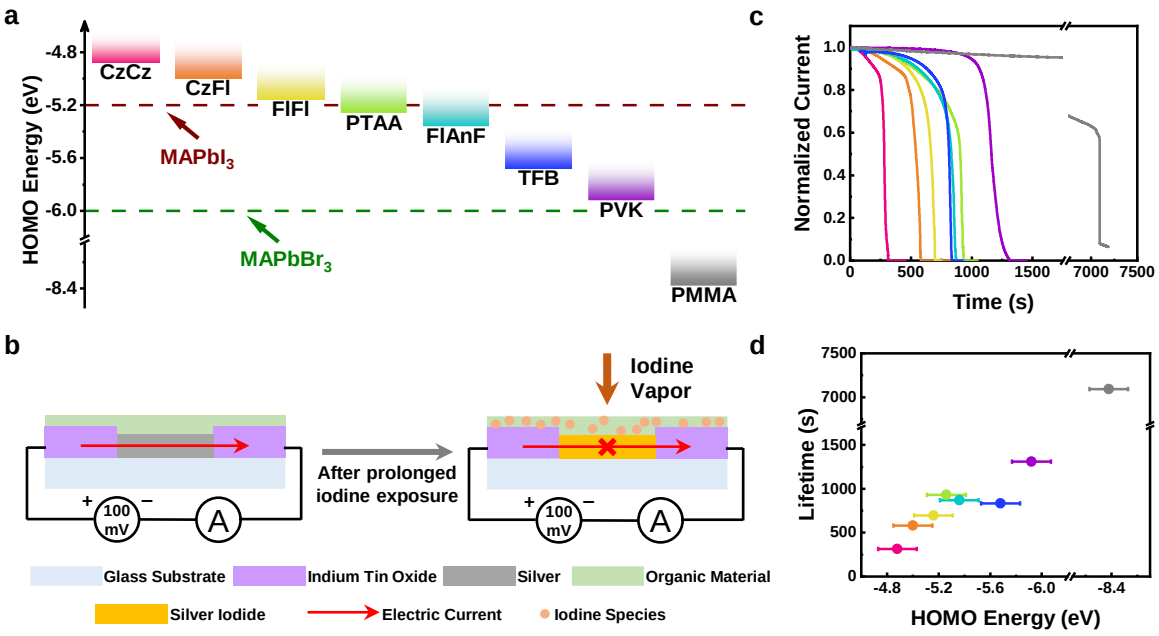

Figure 1. Measured HOMO energies of organic HTLs used in this study with associated Ag:I_2 corrosion rates. (a) HOMO energies of organic HTLs measured by UPS, where the VBM positions of perovskites are marked as the dashed lines. (b) Schematic of the Ag:I_2 corrosion test for evaluating iodine diffusion rates through organic HTL thin films. (c) Normalized current transients of Ag:I_2 corrosion tests with different organic HTLs. (d) Ag resistor lifetime versus HOMO energy of organic HTLs used in the Ag:I_2 corrosion test. The error bars reflect the standard deviation of HOMO energies measured from UPS.

It has been widely reported that I_2 and other mobile oxidized iodine species (e.g., interstitial iodine I_i^+) can form under irradiation,[12, 48, 49] and that the transport of those iodine species play an important role in light-induced halide segregation.[50] Since a high diffusivity of iodine has already been demonstrated in shallow-HOMO organic HTLs,[34] to begin with, we compare iodine transport within organic HTLs employed in this work. In this study, we exclusively test wide gap disordered polymers to minimize effects of morphology and avoid optical excitation of the organic layer. We utilize seven semiconducting polymeric HTLs with differing HOMO levels as well as poly(methyl methacrylate) (PMMA), an insulating polymer with an extremely deep HOMO level as a reference. The molecular structures of each of these polymers are shown

in Figure S1. The HOMO levels of these polymers were measured by ultraviolet photoemission spectroscopy (UPS) shown in Figure S2, Table S1, and Figure 1a, where the reported valence band maximum (VBM) positions of $MAPbI_3$ and $MAPbBr_3$ are also shown for reference.[51] We characterized the iodine diffusion rate through the HTLs using a Ag:I_2 corrosion test, modified from the commonly used Ca corrosion test for characterizing water vapor transmission rate,[52] which is described in detail in our previous study.[34] Figure 1b shows the schematic and the device structure used in the Ag:I_2 corrosion test, which consists of a 100 nm thick Ag thin film resistor as the I_2 sensor, bridging a 5 mm wide channel between prepatterned indium tin oxide (ITO) electrodes. The tested polymers were spin-coated on top of the Ag layer, and to make the comparison reasonable, the thicknesses of different HTLs were measured to be similar (Table S2). During the Ag:I_2 corrosion test, a 100 mV bias was applied to the device and the current was measured as a function of time while it was exposed to I_2 vapor. As iodine transmits through the organic layer, silver is oxidized and converted to insulating silver iodide, cutting off the current. The current transients for different HTLs are shown in Figure 1c, where we can extract the device lifetime (when the current is cut off) for different HTLs shown in Figure 1d. The device lifetime observed in the Ag:I_2 corrosion test directly reflects the diffusion rate of iodine within the organic layer, with a shorter lifetime indicating a faster transmission of iodine through the organic layer. From Figure 1d, we can clearly see a trend that the HTLs with shallower HOMO levels exhibit shorter lifetimes and thus higher diffusion rates for iodine, consistent with findings from our previous study.[34]

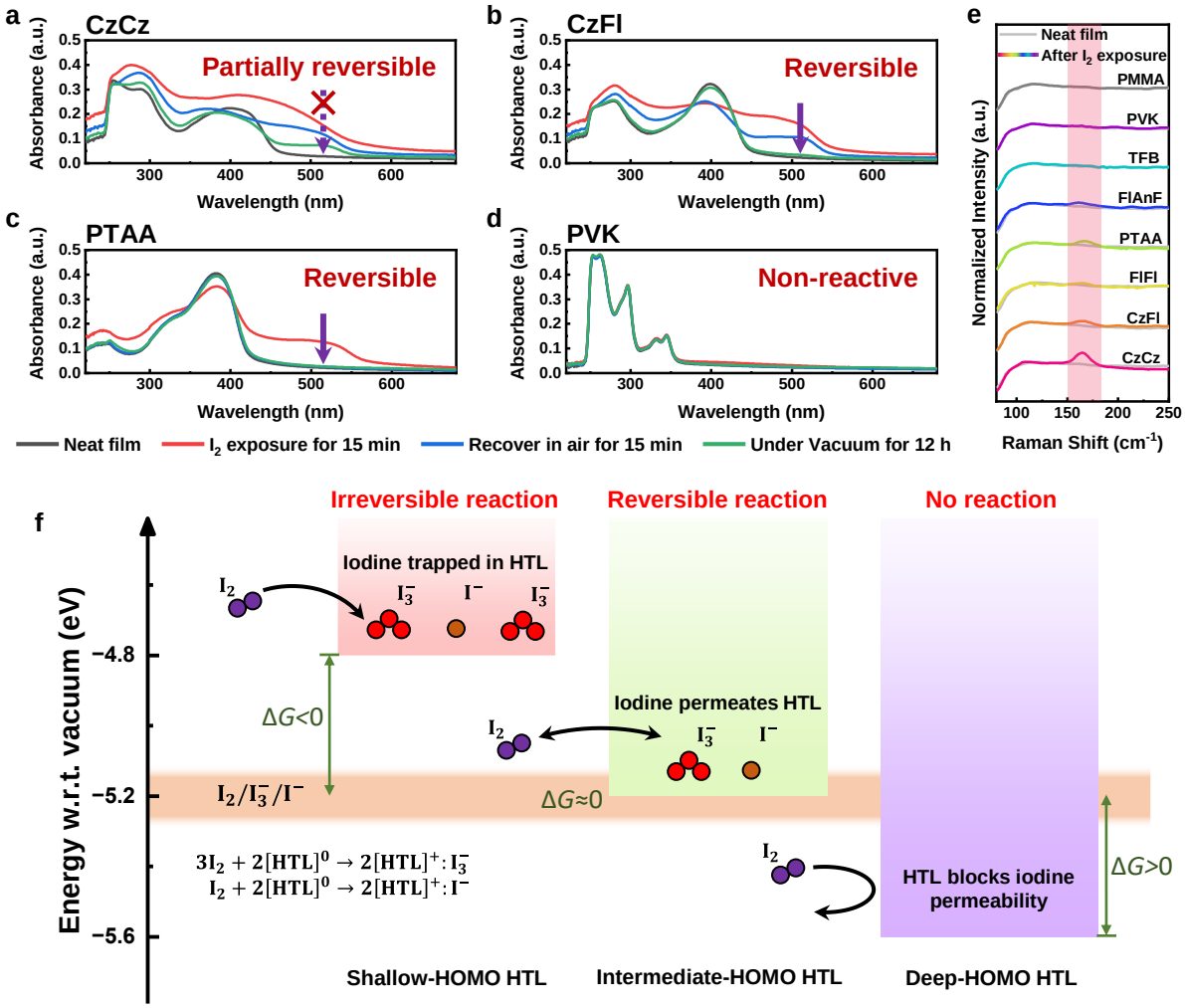

Figure 2. Interaction between I_2 and organic HTLs. (a–d) UV-vis absorption spectra of (a) CzCz, (b) CzFl, (c) PTAA, and (d) PVK thin films collected at different stages before and after I_2 exposure. (e) Raman spectra of the indicated organic HTLs before and after I_2 exposure for 15 min. (f) Schematic of reactions between I_2 and HTLs with different HOMO levels.

We then explored the interaction between I_2 and organic HTLs and its reversibility. Figures 2a–d and S3 show the ultraviolet-visible (UV-vis) absorption spectra of organic HTL films before and after I_2 exposure, followed by recovery processes. For HTLs with relatively shallow HOMO levels (CzCz, CzFl, PTAA, and FlFl), there is a new absorption peak showing up in the 450–550 nm range just following I_2 exposure, which corresponds to cation absorption of $[HTL]^+$ and is consistent with other oxidized HTLs.[34, 53, 54] Such an observation indicates that these shallow-HOMO HTLs can be rapidly oxidized and doped by I_2, which is also the origin of higher I_2 diffusion rate.[34]

Amongst these shallow-HOMO HTLs, CzCz has the shallowest HOMO level and is able to retain such a cation absorption peak even after being pumped under vacuum for 12 h, whereas PTAA, with a deeper HOMO level, can be fully recovered upon exposure to air for 15 min. These results indicate that the strength of reaction between an HTL and I_2 is inversely proportional to the HTL IE, and some HTLs with shallow HOMO level (such as CzCz) can form a quasi-stable salt (i.e., irreversible doping) after I_2 exposure. On the other hand, for HTLs with a relatively deep HOMO level (FlAnF, TFB, PVK, and PMMA), the absorption spectrum barely changes after I_2 exposure, demonstrating weak interaction between I_2 and these materials (i.e., I_2 is an insufficiently strong oxidizer). Figure 2e shows the Raman spectroscopy measurements on these HTLs before and after I_2 exposure. A new peak emerges at approximately 150 to 180 cm^{-1} after I_2 exposure only for shallow-HOMO HTLs (CzCz, CzFl, FlFl, PTAA, and FlAnF), which corresponds to an I–I stretching vibration,[55, 56] resulting from I_2 doping in these shallow-HOMO HTLs.

We further demonstrate that the reactions between I_2 and HTLs result in different products or iodine speciation shown in the diagram shown in Figure 2f, where the difference between IE of HTL and redox potential of iodine/triiodide/iodide provides the thermodynamic driving force (ΔG) of the reaction. First, a HTL with shallow HOMO level, i.e. IE smaller than the redox potential of iodine/triiodide/iodide, can be readily oxidized by I_2. The electrons in the HOMO of the HTL can irreversibly transfer to I_2, forming stable $[\mathrm{HTL}]^+:\mathrm{I}_3^-$ or $[\mathrm{HTL}]^+:\mathrm{I}^-$ compounds, and trapping iodine species in the HTL. When the HTL IE is approximatively resonant with the redox potential of iodine/triiodide/iodide, I_2 can still oxidize and penetrate the HTL, but the reaction is reversible. Finally, for an HTL with a sufficiently deep HOMO level, the redox reaction is cut off owing to the positive ΔG, which effectively blocks the formation of I_3^- and I^- species and slows I_2 permeation in the HTL.

Light-induced halide segregation at perovskite/organic HTL interfaces

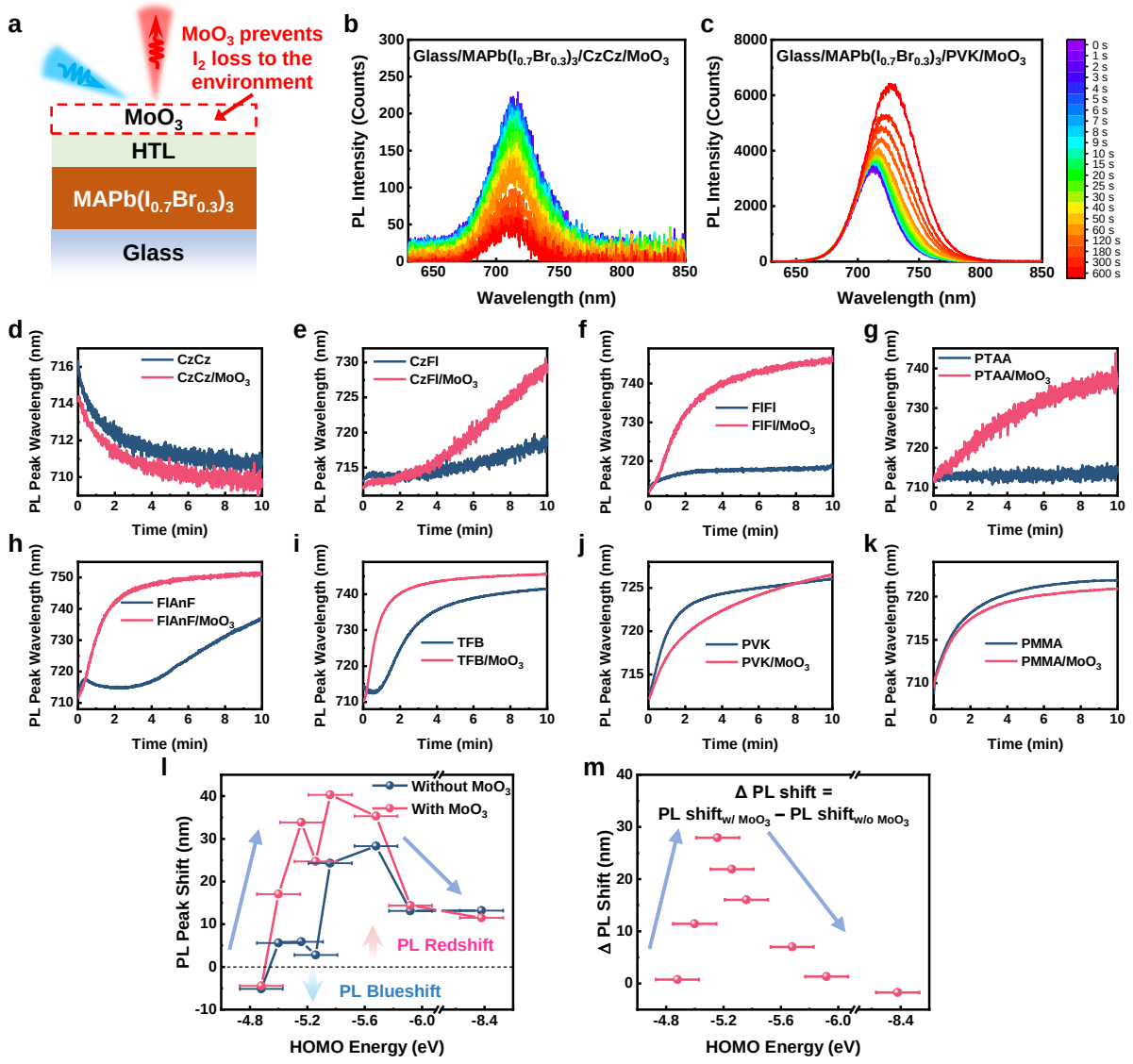

Figure 3. Light-induced halide segregation characterized by PL measurements. (a) Sample structure for PL measurements. (b, c) PL transient measurements on glass/MAPb($I_{0.7}Br_{0.3}$)$_3$/organic HTL/MoO_3 structure under continuous light excitation (450 nm, 20 mW cm^{-2}) over 10 min for (b) CzCz and (c) PVK. (d–k) PL peak wavelength evolution under continuous light excitation (450 nm, 20 mW cm^{-2}) on a mixed-halide perovskite film in contact with different organic HTLs with and without a MoO_3 capping layer: (d) CzCz, (e) CzFl, (f) FlFl, (g) PTAA, (h) FlAnF, (i) TFB, (j) PVK, and (k) PMMA. (l) PL peak wavelength shift after a 10-min PL transient measurement versus HOMO energy of organic HTLs with and without a MoO_3 capping layer. (m) Difference in PL peak shift with and without a MoO_3 capping layer (Δ *PL shift* = *PL peak shift*$_{\text{with MoO3}}$ – *PL peak shift*$_{\text{without MoO3}}$) versus HOMO energy of organic

HTLs. The error bars in (l) and (m) reflect the standard deviation of HOMO energies measured by UPS.

Informed by the understanding of interaction between I_2 and organic HTLs with different HOMO energies, we conducted a series of PL measurements on mixed-halide perovskites in contact with different HTLs to study the effect of HTLs on light-induced halide segregation. To ensure that the perovskite layers have the same quality across different samples and to minimize any morphological effect of different HTLs, all perovskite layers were fabricated directly on glass with the HTL on top. We employed two sample structures with or without a MoO_3 capping layer for PL measurements as shown in Figure 3a. MoO_3 has been demonstrated to be less permeable to iodine species and can thus serve as a good iodine blocking layer to avoid iodine loss into the environment.[34] We optically excited and detected the sample from the HTL side, and monitored the PL emission of the sample over 10 min under continuous 450-nm excitation, which is below the optical gap of all HTLs to avoid parasitic absorption and emission (Figures S4 and S5). Two representative PL spectral evolution measurements using either a shallow-HOMO HTL (CzCz) or a deep-HOMO HTL (PVK) are shown in Figure 3b, c. The PL peak wavelength and peak intensity for different samples were fitted and extracted as a function of illumination time, as plotted in Figures 3d–k and S6 respectively. To assist in the comparison among different HTLs, we plot the PL peak shift after 10 min of continuous illumination for different HTLs with and without a MoO_3 capping layer (which is also a wide-bandgap layer) in Figure 3l, where we can clearly see that the HTL alters the rate of changes in the PL peaks.

A redshifted PL spectrum has been commonly reported as a sign of light-induced halide segregation.[18] However, the first anomalous observation from Figure 3l is that CzCz, the HTL with the most shallow HOMO level of the materials examined here, causes the PL spectrum of mixed-halide perovskite to blueshift, which is less commonly reported for light-induced halide segregation. Another observation is that HTLs with intermediate HOMO energy correspond to the fastest and largest-magnitude PL redshift, i.e. halide segregation, while HTLs with either shallow or deep HOMO levels exhibit slow and minimal PL shifts. This nonmonotonic behavior of the PL peak shift versus HOMO energy demonstrates that the kinetics of halide segregation

are governed by multiple competing processes that have different or opposite rate dependency on the HOMO energy of the organic HTL that is in contact with the mixed-halide perovskite. These subtleties may also account for inconsistent observations in previous studies.[35-39]

Regarding the effect of MoO_3 and iodine blocking, we define Δ *PL shift* as the difference in PL peak shift with and without a MoO_3 capping layer, which can be expressed as *PL peak shift*$_{\text{with MoO3}}$ − *PL peak shift*$_{\text{without MoO3}}$, and we plot Δ *PL shift* as a function of HTL HOMO energy in Figure 3m. We find that Δ *PL shift* is close to zero for both the HTLs with shallow and deep HOMO level, which means MoO_3 negligibly alters the kinetics of halide segregation in these two cases, while for HTLs with intermediate HOMO energy (like FlFl and PTAA), adding a MoO_3 capping layer can greatly increase the rate and extent of the PL redshift, even though MoO_3 is **not** in direct contact with the perovskite layer. Such an observation strongly indicates the importance of irreversible, reversible, and absence of reactions with I_2, as well as the existence of external halide transport pathways, i.e., outside the perovskite layer. In this case, the MoO_3 capping layer, which prohibits the escape of iodine out of the HTLs, most strongly influences halide redistribution in the perovskite layer for HTLs with intermediate HOMO levels and reversible I_2 reactions.

Although many models have been proposed to explain light-induced halide segregation, such as intrinsic thermodynamic instability,[20, 22, 30, 57] polaron-induced or external strain,[23-25, 29, 58] trapping-induced electric field,[27, 37, 59] and carrier density gradient,[21] only a few take HTLs into account but only acknowledge their effect on hole extraction.[35, 38, 39] None of them can explain the nonmonotonic trend of the PL peak shift versus HOMO energy or changes after adding a MoO_3 capping layer, which does not affect the hole extraction. Our experimental results suggest that ionic effects must be taken into account to understand the role of HTLs in light-induced halide segregation.[60, 61]

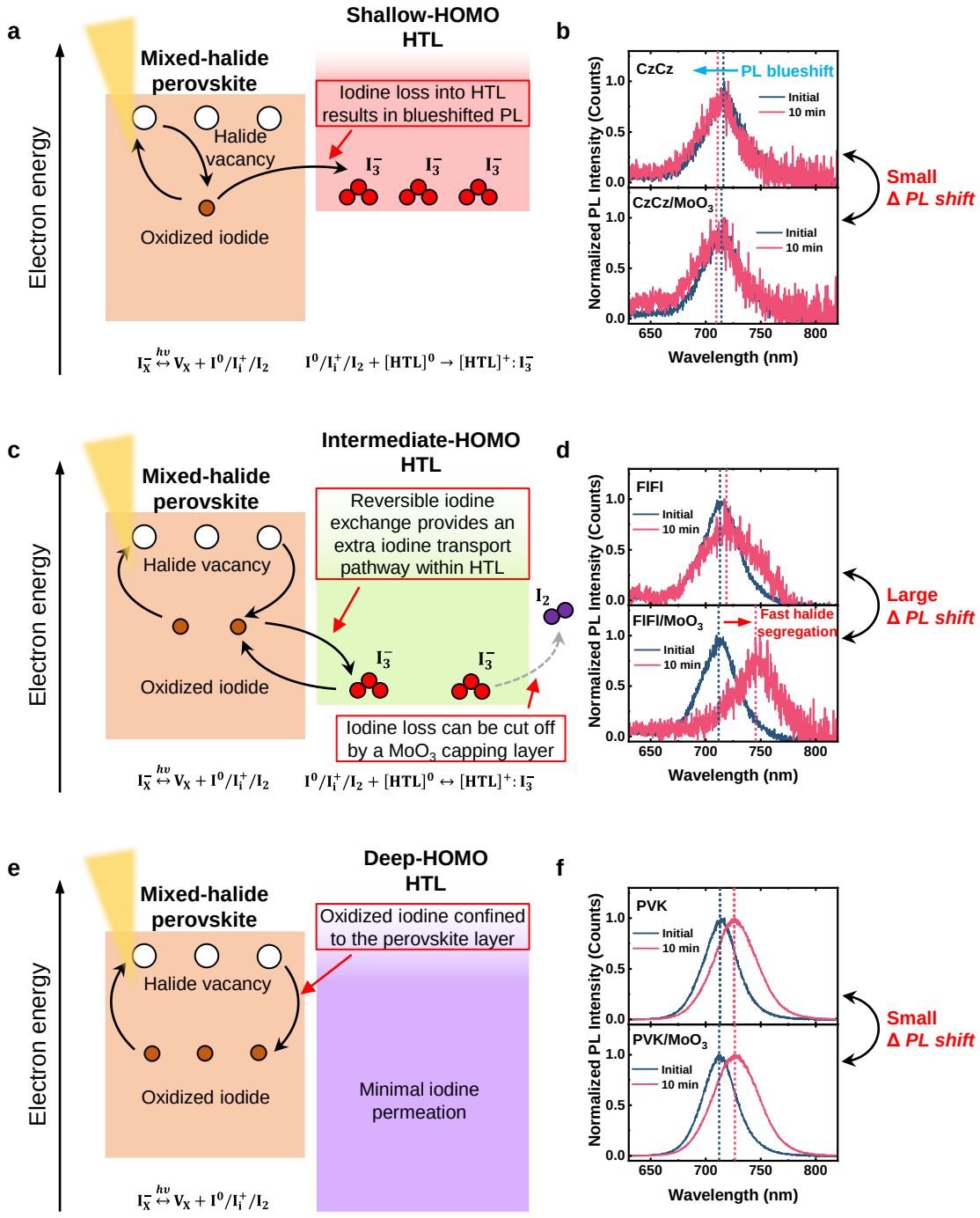

Figure 4. Schematic of light-induced halide segregation for mixed-halide perovskite in contact with different organic HTLs. (a) Iodine transport pathways in a mixed-halide perovskite/shallow-HOMO HTL stack under illumination. (b) PL spectra before and after 10-min illumination on a glass/MAPb($I_{0.7}Br_{0.3}$)$_3$/CzCz stack with and without a MoO_3 capping layer. (c) Iodine transport pathways in a mixed-halide perovskite/intermediate-HOMO HTL stack under illumination. (d) PL spectra before and after 10-min illumination on a glass/MAPb($I_{0.7}Br_{0.3}$)$_3$/FlFl stack with and without a MoO_3 capping layer. (e) Iodine transport

pathways in a mixed-halide perovskite/deep-HOMO HTL stack under illumination. (f) PL spectra before and after 10-min illumination on a glass/MAPb($I_{0.7}Br_{0.3}$)$_3$/PVK stack with and without a MoO_3 capping layer. Excitation is provided by a 450-nm laser diode (20 mW cm^{-2}) in (b), (d), and (f) and the dotted lines indicate the fitted peak position of the PL spectrum.

To fully elucidate the observations from PL measurements and understand the effect of the HTL on light-induced halide segregation, we first look retrospectively at our previous study, where we proposed a photoelectrochemical model to rationalize halide segregation under general external stressors.[50] For the case of light-induced halide segregation, selective iodide photo-oxidation initiates the unbalanced iodine and bromine migration, leading to halide redistribution and segregation. In this case, the transport of oxidized iodide plays an important role in initiating the whole process and greatly affects the kinetics of halide segregation. By further combining characterizations on I_2:HTL interactions and observations from PL transient measurements, we presume that HTLs can change the kinetics of halide segregation by affecting the oxidized iodide transport pathways, where HTLs with different HOMO levels have different effects on multiple pathways, leading to nonmonotonic trends observed in PL transients.

Herein, we provide schematic diagrams illustrating iodine transport pathways at perovskite/organic HTL interfaces for three different cases in Figure 4. A more detailed kinetic analysis to account for all the key observations in PL measurements is discussed in Figure S7. First, for shallow HOMO HTLs, the oxidized iodine resulting from light excitation will be trapped in the HTL (Figure 4a) as demonstrated in UV-vis measurements shown in Figure 2, which competes with the halide segregation and iodide-rich domain formation in the perovskite layer. For an HTL with a shallow HOMO level, the amount of iodine trapped in the HTL appears to be so large that it produces a bromide-rich composition and thus a PL blueshift. This explains the abnormal PL blueshift observed in the CzCz samples as shown in Figure 4b. Such a PL blueshift has also been observed in previous studies and ascribed to iodide loss from the perovskite sample,[62-64] which is consistent with our model. Furthermore, since the iodine species can be stably trapped in the HTL without escaping into the environment, adding a MoO_3 capping layer does not change the established iodine transport pathways, which accounts for

the negligible Δ *PL shift*.

For HTLs with an intermediate HOMO level, there is still a moderate amount of iodine diffusion through the HTL, which provides an extra iodine transport pathway within the HTL. In this case, less iodine is trapped in the HTL, and it may reversibly exchange with the perovskite layer as well as escape from the HTL into the environment. The extra iodine transport pathway within the HTL is more efficient compared to the iodine transport through the bulk of the perovskite film in the form of interstitial iodine (I_i), which is relatively slow due to a low diffusion coefficient of I_i in the absence of structural defects and halide vacancies.[50] This contributes to the fastest halide segregation as shown in Figure 4d. At the same time, adding a MoO_3 capping layer can greatly influence the iodine transport pathways by blocking iodine loss, which accounts for a large Δ *PL shift* in this case. Finally, for the HTL with a deep HOMO level, the diffusion rate is low for oxidized iodide into the HTL and iodine can only transport through the bulk of the perovskite, causing a relatively slow halide segregation and also a small Δ *PL shift*.

Light-induced PL quenching and enhancement at perovskite/organic HTL interfaces

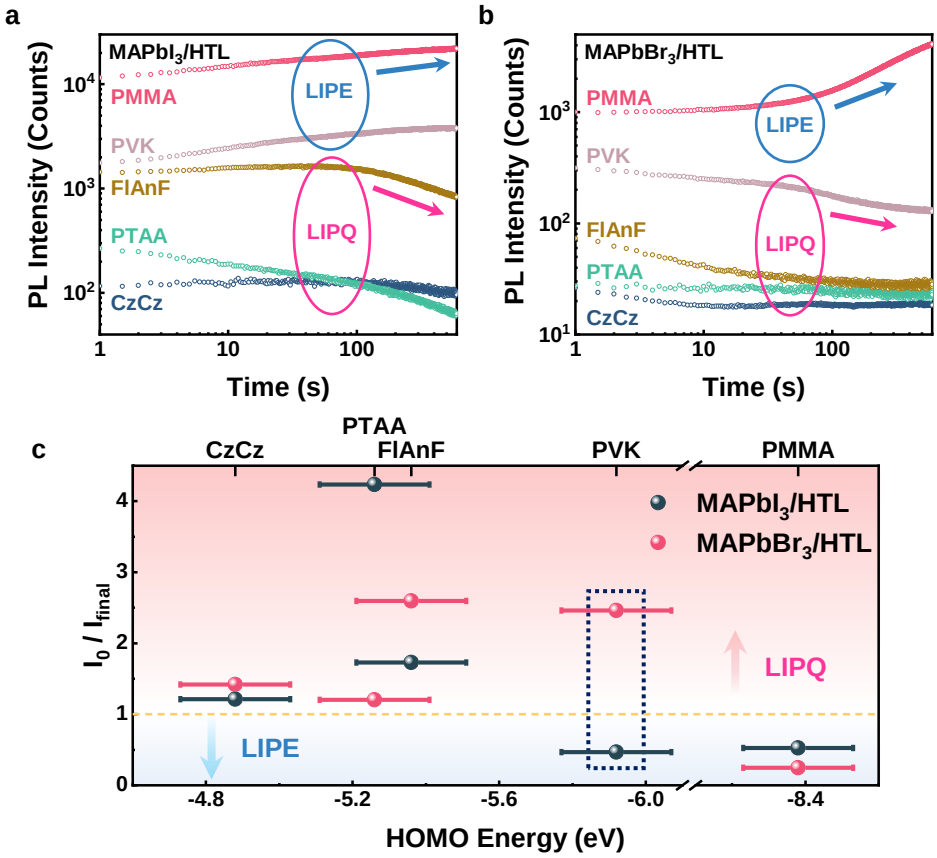

Figure 5. Light-induced PL quenching and enhancement at pure-halide perovskite/organic HTL interfaces. (a, b) PL intensity evolution under continuous light excitation (450 nm, 20 mW cm^{-2}) on (a) a glass/$MAPbI_3$/organic HTL/MoO_3 stack and (b) a glass/$MAPbBr_3$/organic HTL/MoO_3 stack. (c) The ratio of initial PL intensity (I_0) to PL intensity at the end of the 600 s transient measurement (I_{final}) versus HOMO energy of the organic HTL. The error bars reflect the standard deviation of HOMO energies measured from UPS.

Besides the PL spectral shift resulting from light-induced halide segregation, another instability in the PL that involves intensity change is also observed under constant illumination, which affects all perovskite compositions including single-halide ones. Compared to LIPE, which has been observed in isolated neat perovskite samples,[40-42] we also observe LIPQ, a detrimental process for device applications, as it directly reflects an increase in non-radiative recombination. Herein, we use pure-halide perovskites to study the effect of HTLs on the PL intensity change over time to avoid ambiguity introduced by halide segregation induced carrier

funneling effect. We conducted similar PL transient measurements on glass/$MAPbI_3$/organic HTL/MoO_3 and glass/$MAPbBr_3$/organic HTL/MoO_3 structures (Figures S8 and S9), and plot the PL peak intensity as a function of illumination time in Figure 5a, b.

Our first observation is that for both $MAPbI_3$ and $MAPbBr_3$ samples, the initial PL intensity (I_0) of stacks with different HTLs follows the trend of the HOMO energy, i.e., the HTL with a deeper HOMO level shows a higher I_0 and less PL quenching; the same trend of I_0 is also observed for the mixed-halide compositions (Figures S4–S6). Beyond the trend of initial PL quenching, which is commonly used to invoke the ability of charge extraction,[44-47] we further compare the change of PL intensity during continuous illumination. We calculate the ratio between I_0 and the PL intensity after 10-min illumination (I_{final}) to reflect the change in PL intensity. A higher than unity value of I_0/I_{final} indicates LIPQ, while a lower than unity value of I_0/I_{final} indicates LIPE. The I_0/I_{final} values for different samples are plotted in Figure 5c, where we observe that samples with shallow-HOMO HTLs (CzCz, PTAA, and FlAnF) show LIPQ while the sample with deep-HOMO HTL (PMMA) shows LIPE. Most interestingly, for the samples with intermediate-HOMO HTL (PVK), the $MAPbI_3$ sample shows LIPQ while the $MAPbBr_3$ instead shows LIPE, which strengthens our conclusion that the primary reaction affecting PL transients and quenching involves halogen:HTL redox reactions dictated by the HTL HOMO energy and iodine/triiodide/iodide (or bromine/tribromide/bromide) redox potentials.

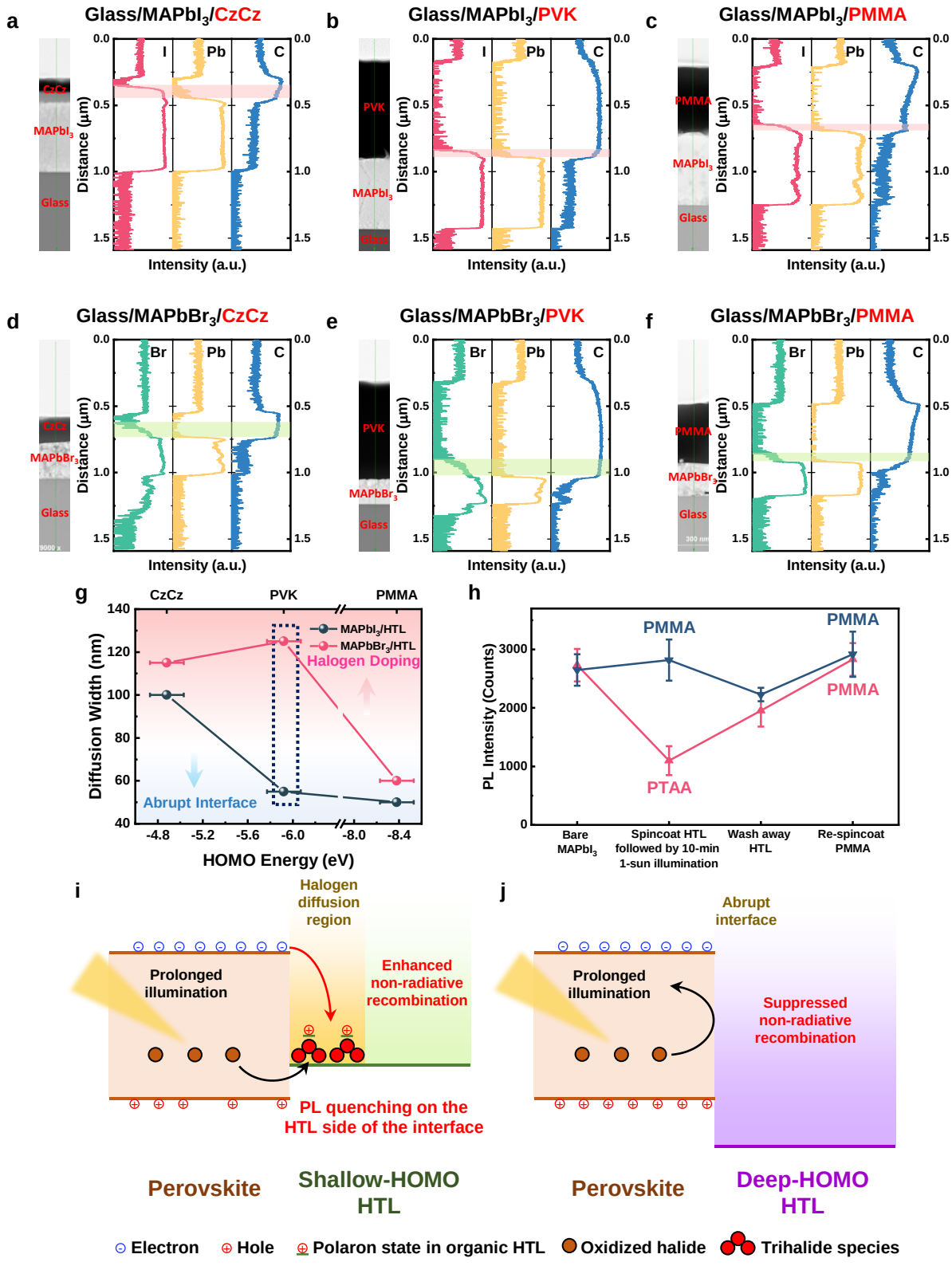

Figure 6. Origin of light-induced PL quenching at pure-halide perovskite/organic HTL interfaces. (a–f) cross-sectional STEM-EDX measurement on (a) a glass/$MAPbI_3$/CzCz stack, (b) a glass/$MAPbI_3$/PVK stack, (c) a glass/$MAPbI_3$/PMMA stack, (d) a glass/$MAPbBr_3$/CzCz stack, (e) a glass/$MAPbBr_3$/PVK stack, (f) a glass/$MAPbBr_3$/PMMA stack after AM 1.5 G light

soaking for 12 h. The color-shaded bands reflect the halogen diffusion from perovskite into organic HTL. (g) The width of the halogen diffusion region into the HTL versus HTL HOMO energy. The error bars reflect the standard deviation of HOMO energies measured from UPS. (h) PL intensity of two identical glass/$MAPbI_3$ samples followed by different treatments at different stages. The error bars reflect the standard deviation of PL intensity measured from five different spots on one sample. (i, j) Schematic of perovskite/organic HTL interfaces after prolonged illumination for (i) a shallow-HOMO HTL and (j) a deep-HOMO HTL.

To understand the different PL behaviors under continuous illumination, we conducted cross-sectional STEM-EDX measurements on both glass/$MAPbI_3$/organic HTL and glass/$MAPbBr_3$/organic HTL structures with either a shallow-HOMO (CzCz), intermediate-HOMO (PVK), or a deep-HOMO material (PMMA) after prolonged illumination, and show results in Figure 6a–f. By comparing the halogen and lead elemental profiles at the perovskite/HTL interface, we find that both halogen species can diffuse from the perovskite into the HTL, but the extent of halogen diffusion varies. To quantify the degree of halogen diffusion, we define the width of halogen diffusion as the distance between the onsets of the halogen and lead elemental profiles in STEM-EDX, which are marked as the color-shaded bands in Figure 6a–f. From the diffusion width of halogen species into the HTL (Figure 6g). We find that: for samples with a shallow-HOMO HTL (CzCz), both iodine and bromine show a similar and large diffusion width; for samples with a deep-HOMO HTL (PMMA), both show a similarly small diffusion width, indicating a relatively abrupt interface; however, for samples with an intermediate-HOMO HTL (PVK), the $MAPbI_3$ sample shows a relatively abrupt interface while the $MAPbBr_3$ shows substantial bromine diffusion. The difference in the halogen diffusion width into PVK between $MAPbI_3$ and $MAPbBr_3$ samples can be rationalized by the fact that bromine/tribromide/bromide has a deeper redox potential than that of iodine/triiodide/iodide.[65] Thus, oxidized bromide is capable of oxidizing/doping HTLs with deeper HOMO energies like PVK. This leads to the conclusion that PVK only favors bromine diffusion via a redox reaction,[34] and the iodide pathway being electrochemically inaccessible for this configuration (i.e. iodine cannot dope PVK as established in Figure 2).

The observations in STEM-EDX measurements (Figure 6g) mimics the trend seen in PL transient measurements (Figure 5c), where an interface with severe halogen diffusion corresponds to LIPQ while an abrupt interface is associated with LIPE, indicating a correlation between a halogen diffusion layer at the perovskite/organic HTL interface and PL quenching. Furthermore, to explore whether LIPQ originates from diffused halogen species in the HTL or halide vacancies remaining in the perovskite due to halogen loss (i.e. whether carriers are quenched on the perovskite or HTL side of the interface), we performed a series of steady-state PL measurements as shown in Figure 6h. We started from two identical $MAPbI_3$ samples, which show similar PL intensities, and spin-coated a layer of either PTAA or PMMA on top followed by 10-min 1-sun illumination. The PTAA sample shows substantially decreased PL intensity while the PMMA sample shows a slightly enhanced PL, consistent with Figure 5c. Then, we washed away both HTLs and spin-coated a fresh layer of PMMA for each sample, and we find that the PL intensity of the PTAA sample is recovered and close to that of the original PMMA sample. The reversible PL in the PTAA sample demonstrates that non-radiative recombination at the perovskite/organic HTL interface originates from halogen species and/or the organic polaron formed on the HTL-side of the interface, rather than increased halide vacancies or any other changes in the perovskite layer due to halogen loss.

The LIPE observed in both $MAPbI_3$/PMMA and $MAPbBr_3$/PMMA samples (used as references since PMMA forms an inert interface with the perovskite with negligible charge transfer) indicate that LIPE may be ascribed to a bulk effect of the perovskite and is not directly related to the perovskite/organic HTL interface, which is thus beyond the scope of this paper and has been discussed in the literature.[40, 49] The LIPQ observed in this study, which we showed is a direct result of iodine on the organic HTL-side of the interface, happens on the timescale of minutes, and cannot be explained by the charge extraction effect (a purely electronic process with a timescale of fs to ns, and then reaches steady state) as commonly reported in the literature for PL quenching.[44-47] Instead, an ionic process must be involved in this slow transient. In fact, since a good hole extraction layer that does not lead to non-radiative recombination should not quench carriers,[66] carrier extraction on its own is insufficient to explain PL quenching. Combining the observations from PL and STEM-EDX measurements discussed above, we can

obtain a comprehensive picture of halogen diffusion at perovskite/organic HTLs and its effect on LIPQ, and the schematic is shown in Figure 6i, j. First, when perovskite is in contact with an HTL with a shallow HOMO level (Figure 6i), light excitation can oxidize the halide species in the perovskite and form mobile interstitial halogen or even halogen vapor; those oxidized halide species can then diffuse into and dope the HTL to form a stable interfacial doping region (color-shaded bands in Figure 6a–f) with an increased polaron density. Such an interfacial doping region serves as a non-radiative recombination center, and the hole polarons in this region can non-radiatively recombine with electrons from the perovskite, thereby quenching PL. The rate of non-radiative recombination is proportional to the density of electrons in the perovskite (which changes negligibly over time) and the density of hole polarons in the HTL. During continuous light illumination, an increasing number of halide species will be oxidized and dope the HTL, thus leading to a higher polaron population (compensated by halide anions to ensure charge neutrality) in the interfacial doping region, which becomes a more effective non-radiative recombination center over time and causes LIPQ. On the other hand, the HTL with a deep HOMO level suppresses halogen diffusion and forms an abrupt interface with the perovskite (Figure 6j), and even if there is any initial hole transfer from perovskite to HTL, an electric field will quickly build up in the space charge region to avoid further accumulation of holes in the HTL. Such an abrupt interface changes negligibly under illumination and thus does not quench PL over time.

Finally, this comprehensive picture provides deeper insight into our previous study on perovskite solar cell performance using a similar set of organic HTLs.[67] In particular, the open-circuit voltage (V_{OC}) of mixed iodide/bromide perovskite solar cells is observed to increase as the HTL HOMO level becomes deeper up to ~-5.1 eV, which corresponds to a similar level where we observe HTL/iodine reactions to slow significantly, but then plateaus for even deeper HOMO energies. Our results here demonstrate that non-radiative recombination is dominated by the iodine-doped HTL region for shallower HOMO levels, where the interfacial non-radiative recombination limits V_{OC}. Further gains in V_{OC} are not observed for deeper HOMO energies, suggesting the interfacial non-radiative recombination decreases as the iodine/HTL reactions become less severe, and V_{OC} becomes limited by non-radiative recombination in the

bulk perovskite or at a different interface.

Conclusions

In summary, we systematically study iodine transport and doping in organic HTLs and demonstrate that the HOMO energy of the HTL dictates the reactivity and reversibility of iodine doping. By employing a series of organic HTLs with different HOMO levels, we investigate the effect of the HTL on the PL behavior at perovskite/organic HTL interfaces, including light-induced halide segregation and PL intensity changes (LIPQ and LIPE) over time. We demonstrate the existence of iodine transport pathways *outside the perovskite layer* can strongly influence light-induced halide segregation, which are enabled by HTLs with sufficiently shallow HOMO energy, confirming the key role of iodine mass transport in light-induced halide segregation. We further assert a connection between halogen diffusion and non-radiative recombination, clarifying the origin of light-induced PL quenching at perovskite/organic HTL interfaces. All PL phenomena can be rationalized by considering halogen loss pathways from the perovskite layer, together with subsequent interactions with HTLs, ultimately determined by the HTL HOMO energy and the redox potentials of halogens. These findings again highlight that halogen oxidation and diffusion within perovskite devices is one of the main culprits of degradation, and also provide guidelines for the design of HTLs with suitable HOMO levels to mitigate halogen diffusion. Furthermore, effective halogen (mainly iodine for most commonly used compositions) blocking strategies are still required to fully suppress this degradation and non-radiative recombination pathway.

Associated Content

Supporting Information

The Supporting Information is available free of charge at https://pubs.acs.org.

Experimental details (including materials used in this study, synthesis of polymeric HTLs, sample fabrication methods, and characterizations); chemical structure of the HTLs, UPS measurements; UV-vis absorption measurements; PL transient measurements; supplementary discussion of light-induced halide segregation; HOMO energy of the HTLs; and thickness of the HTLs.

Notes

The authors declare no competing interests.

Acknowledgements

We acknowledge funding for this work by the Department of the Navy, Office of Naval Research under ONR award number N00014-21-1-2767. This work was authored in part by the National Renewable Energy Laboratory, operated by Alliance for Sustainable Energy, LLC, for the U.S. Department of Energy (DOE) under Contract No. DE-AC36-08GO28308. Funding for R.A.K., K.Z., and J.J.B. was provided by U.S. Department of Energy, Office of Energy Efficiency and Renewable Energy, Solar Energy Technologies Office (SETO) project "Advanced Perovskite Cells and Modules" program (DE-FOA-0000990). A.S. and D.D.A. acknowledge support by the U.S. Department of Energy, Office of Energy Efficiency and Renewable Energy, Solar Energy Technologies Office by Award Number DE-EE0008978. X.Z. and A.K. acknowledge support by the US-Israel Binational Science Foundation (Grant No. 2018349). The views expressed in the article do not necessarily represent the views of the DOE or the U.S. Government. The U.S. Government retains and the publisher, by accepting the article for publication, acknowledges that the U.S. Government retains a nonexclusive, paid-up, irrevocable, worldwide license to publish or reproduce the published form of this work, or allow others to do so, for U.S. Government purposes. The authors acknowledge the use of Princeton's Imaging and Analysis Center (IAC), which is partially supported by the Princeton Center for

Complex Materials (PCCM), a National Science Foundation (NSF) Materials Research Science and Engineering Center (MRSEC; DMR-2011750).

References

(1) Zhou, Y.; Herz, L. M.; Jen, A. K. Y.; Saliba, M. Advances and Challenges in Understanding the Microscopic Structure–Property–Performance Relationship in Perovskite Solar Cells. *Nat. Energy* **2022,** *7* (9), 794-807.

(2) Huang, J.; Yuan, Y.; Shao, Y.; Yan, Y. Understanding the Physical Properties of Hybrid Perovskites for Photovoltaic Applications. *Nat. Rev. Mater.* **2017,** *2* (7), 17042.

(3) Tan, Z.-K.; Moghaddam, R. S.; Lai, M. L.; Docampo, P.; Higler, R.; Deschler, F.; Price, M.; Sadhanala, A.; Pazos, L. M.; Credgington, D.; Hanusch, F.; Bein, T.; Snaith, H. J.; Friend, R. H. Bright Light-Emitting Diodes Based on Organometal Halide Perovskite. *Nat. Nanotechnol.* **2014,** *9* (9), 687-692.

(4) Xing, G.; Mathews, N.; Lim, S. S.; Yantara, N.; Liu, X.; Sabba, D.; Grätzel, M.; Mhaisalkar, S.; Sum, T. C. Low-Temperature Solution-Processed Wavelength-Tunable Perovskites for Lasing. *Nat. Mater.* **2014,** *13* (5), 476-480.

(5) Dou, L.; Yang, Y.; You, J.; Hong, Z.; Chang, W.-H.; Li, G.; Yang, Y. Solution-Processed Hybrid Perovskite Photodetectors with High Detectivity. *Nat. Commun.* **2014,** *5* (1), 5404.

(6) Kojima, A.; Teshima, K.; Shirai, Y.; Miyasaka, T. Organometal Halide Perovskites as Visible-Light Sensitizers for Photovoltaic Cells. *J. Am. Chem. Soc.* **2009,** *131* (17), 6050-6051.

(7) Liu, M.; Johnston, M. B.; Snaith, H. J. Efficient Planar Heterojunction Perovskite Solar Cells by Vapour Deposition. *Nature* **2013,** *501* (7467), 395-398.

(8) Min, H.; Lee, D. Y.; Kim, J.; Kim, G.; Lee, K. S.; Kim, J.; Paik, M. J.; Kim, Y. K.; Kim, K. S.; Kim, M. G.; Shin, T. J.; Il Seok, S. Perovskite Solar Cells with Atomically Coherent Interlayers on SnO_2 Electrodes. *Nature* **2021,** *598* (7881), 444-450.

(9) Boyd, C. C.; Cheacharoen, R.; Leijtens, T.; McGehee, M. D. Understanding Degradation Mechanisms and Improving Stability of Perovskite Photovoltaics. *Chem.*

Rev. **2019,** *119* (5), 3418-3451.

(10) Huang, J.; Tan, S.; Lund, P. D.; Zhou, H. Impact of H_2O on Organic–Inorganic Hybrid Perovskite Solar Cells. *Energy Environ. Sci.* **2017,** *10* (11), 2284-2311.

(11) Wei, J.; Wang, Q.; Huo, J.; Gao, F.; Gan, Z.; Zhao, Q.; Li, H. Mechanisms and Suppression of Photoinduced Degradation in Perovskite Solar Cells. *Adv. Energy Mater.* **2021,** *11* (3), 2002326.

(12) Kundu, S.; Kelly, T. L. In Situ Studies of the Degradation Mechanisms of Perovskite Solar Cells. *EcoMat* **2020,** *2* (2), e12025.

(13) Bella, F.; Griffini, G.; Correa-Baena, J.-P.; Saracco, G.; Grätzel, M.; Hagfeldt, A.; Turri, S.; Gerbaldi, C. Improving Efficiency and Stability of Perovskite Solar Cells with Photocurable Fluoropolymers. *Science* **2016,** *354* (6309), 203-206.

(14) Cheacharoen, R.; Boyd, C. C.; Burkhard, G. F.; Leijtens, T.; Raiford, J. A.; Bush, K. A.; Bent, S. F.; McGehee, M. D. Encapsulating Perovskite Solar Cells to Withstand Damp Heat and Thermal Cycling. *Sustain. Energy Fuels* **2018,** *2* (11), 2398-2406.

(15) Ma, S.; Yuan, G.; Zhang, Y.; Yang, N.; Li, Y.; Chen, Q. Development of Encapsulation Strategies Towards the Commercialization of Perovskite Solar Cells. *Energy Environ. Sci.* **2022,** *15* (1), 13-55.

(16) Kirchartz, T.; Márquez, J. A.; Stolterfoht, M.; Unold, T. Photoluminescence-Based Characterization of Halide Perovskites for Photovoltaics. *Adv. Energy Mater.* **2020,** *10* (26), 1904134.

(17) Hoke, E. T.; Slotcavage, D. J.; Dohner, E. R.; Bowring, A. R.; Karunadasa, H. I.; McGehee, M. D. Reversible Photo-Induced Trap Formation in Mixed-Halide Hybrid Perovskites for Photovoltaics. *Chem. Sci.* **2015,** *6* (1), 613-617.

(18) Brennan, M. C.; Ruth, A.; Kamat, P. V.; Kuno, M. Photoinduced Anion Segregation in Mixed Halide Perovskites. *Trends Chem.* **2020,** *2* (4), 282-301.

(19) DuBose, J. T.; Kamat, P. V. Hole Trapping in Halide Perovskites Induces Phase Segregation. *Acc. Chem. Res.* **2022,** *3* (7), 761-771.

(20) Brivio, F.; Caetano, C.; Walsh, A. Thermodynamic Origin of Photoinstability in the $CH_3NH_3Pb(I_{1-x}Br_x)_3$ Hybrid Halide Perovskite Alloy. *J. Phys. Chem. Lett.* **2016,** *7* (6),

1083-1087.

(21) Barker, A. J.; Sadhanala, A.; Deschler, F.; Gandini, M.; Senanayak, S. P.; Pearce, P. M.; Mosconi, E.; Pearson, A. J.; Wu, Y.; Srimath Kandada, A. R.; Leijtens, T.; De Angelis, F.; Dutton, S. E.; Petrozza, A.; Friend, R. H. Defect-Assisted Photoinduced Halide Segregation in Mixed-Halide Perovskite Thin Films. *ACS Energy Lett.* **2017,** *2* (6), 1416-1424.

(22) Draguta, S.; Sharia, O.; Yoon, S. J.; Brennan, M. C.; Morozov, Y. V.; Manser, J. S.; Kamat, P. V.; Schneider, W. F.; Kuno, M. Rationalizing the Light-Induced Phase Separation of Mixed Halide Organic–Inorganic Perovskites. *Nat. Commun.* **2017,** *8* (1), 200.

(23) Bischak, C. G.; Hetherington, C. L.; Wu, H.; Aloni, S.; Ogletree, D. F.; Limmer, D. T.; Ginsberg, N. S. Origin of Reversible Photoinduced Phase Separation in Hybrid Perovskites. *Nano Lett.* **2017,** *17* (2), 1028-1033.

(24) Bischak, C. G.; Wong, A. B.; Lin, E.; Limmer, D. T.; Yang, P.; Ginsberg, N. S. Tunable Polaron Distortions Control the Extent of Halide Demixing in Lead Halide Perovskites. *J. Phys. Chem. Lett.* **2018,** *9* (14), 3998-4005.

(25) Wang, X.; Ling, Y.; Lian, X.; Xin, Y.; Dhungana, K. B.; Perez-Orive, F.; Knox, J.; Chen, Z.; Zhou, Y.; Beery, D.; Hanson, K.; Shi, J.; Lin, S.; Gao, H. Suppressed Phase Separation of Mixed-Halide Perovskites Confined in Endotaxial Matrices. *Nat. Commun.* **2019,** *10* (1), 695.

(26) Beal, R. E.; Hagström, N. Z.; Barrier, J.; Gold-Parker, A.; Prasanna, R.; Bush, K. A.; Passarello, D.; Schelhas, L. T.; Brüning, K.; Tassone, C. J.; Steinrück, H.-G.; McGehee, M. D.; Toney, M. F.; Nogueira, A. F. Structural Origins of Light-Induced Phase Segregation in Organic-Inorganic Halide Perovskite Photovoltaic Materials. *Matter* **2020,** *2* (1), 207-219.

(27) Knight, A. J.; Wright, A. D.; Patel, J. B.; McMeekin, D. P.; Snaith, H. J.; Johnston, M. B.; Herz, L. M. Electronic Traps and Phase Segregation in Lead Mixed-Halide Perovskite. *ACS Energy Lett.* **2019,** *4* (1), 75-84.

(28) Mao, W.; Hall, C. R.; Bernardi, S.; Cheng, Y.-B.; Widmer-Cooper, A.; Smith, T. A.; Bach,

U. Light-Induced Reversal of Ion Segregation in Mixed-Halide Perovskites. *Nat. Mater.* **2021,** *20* (1), 55-61.

(29) Zhao, Y.; Miao, P.; Elia, J.; Hu, H.; Wang, X.; Heumueller, T.; Hou, Y.; Matt, G. J.; Osvet, A.; Chen, Y.-T.; Tarragó, M.; de Ligny, D.; Przybilla, T.; Denninger, P.; Will, J.; Zhang, J.; Tang, X.; Li, N.; He, C.; Pan, A.; Meixner, A. J.; Spiecker, E.; Zhang, D.; Brabec, C. J. Strain-Activated Light-Induced Halide Segregation in Mixed-Halide Perovskite Solids. *Nat. Commun.* **2020,** *11* (1), 6328.

(30) Chen, Z.; Brocks, G.; Tao, S.; Bobbert, P. A. Unified Theory for Light-Induced Halide Segregation in Mixed Halide Perovskites. *Nat. Commun.* **2021,** *12* (1), 2687.

(31) Guo, Y.; Yin, X.; Liu, J.; Que, W. Focusing on Mixed-Halide Br-Rich Perovskite Solar Cells: An Inevitable Open-Circuit Voltage Deficit Derived from Photoinduced Halide Segregation? *Matter* **2022,** *5* (7), 2015-2030.

(32) Xu, Z.; Kerner, R. A.; Berry, J. J.; Rand, B. P. Iodine Electrochemistry Dictates Voltage-Induced Halide Segregation Thresholds in Mixed-Halide Perovskite Devices. *Adv. Funct. Mater.* **2022,** *32* (33), 2203432.

(33) Xu, Z.; Kerner, R. A.; Harvey, S. P.; Zhu, K.; Berry, J. J.; Rand, B. P. Halogen Redox Shuttle Explains Voltage-Induced Halide Redistribution in Mixed-Halide Perovskite Devices. *ACS Energy Lett.* **2023,** *8* (1), 513-520.

(34) Kerner, R. A.; Heo, S.; Roh, K.; MacMillan, K.; Larson, B. W.; Rand, B. P. Organic Hole Transport Material Ionization Potential Dictates Diffusion Kinetics of Iodine Species in Halide Perovskite Devices. *ACS Energy Lett.* **2021,** *6* (2), 501-508.

(35) Lin, Y.; Chen, B.; Fang, Y.; Zhao, J.; Bao, C.; Yu, Z.; Deng, Y.; Rudd, P. N.; Yan, Y.; Yuan, Y.; Huang, J. Excess Charge-Carrier Induced Instability of Hybrid Perovskites. *Nat. Commun.* **2018,** *9* (1), 4981.

(36) Peña-Camargo, F.; Caprioglio, P.; Zu, F.; Gutierrez-Partida, E.; Wolff, C. M.; Brinkmann, K.; Albrecht, S.; Riedl, T.; Koch, N.; Neher, D.; Stolterfoht, M. Halide Segregation Versus Interfacial Recombination in Bromide-Rich Wide-Gap Perovskite Solar Cells. *ACS Energy Lett.* **2020**, 2728-2736.

(37) Belisle, R. A.; Bush, K. A.; Bertoluzzi, L.; Gold-Parker, A.; Toney, M. F.; McGehee, M.

D. Impact of Surfaces on Photoinduced Halide Segregation in Mixed-Halide Perovskites. *ACS Energy Lett.* **2018,** *3* (11), 2694-2700.

(38) DuBose, J. T.; Kamat, P. V. TiO_2-Assisted Halide Ion Segregation in Mixed Halide Perovskite Films. *J. Am. Chem. Soc.* **2020,** *142* (11), 5362-5370.

(39) Lim, V. J. Y.; Knight, A. J.; Oliver, R. D. J.; Snaith, H. J.; Johnston, M. B.; Herz, L. M. Impact of Hole-Transport Layer and Interface Passivation on Halide Segregation in Mixed-Halide Perovskites. *Adv. Funct. Mater.* **2022,** *32* (41), 2204825.

(40) Andaji-Garmaroudi, Z.; Anaya, M.; Pearson, A. J.; Stranks, S. D. Photobrightening in Lead Halide Perovskites: Observations, Mechanisms, and Future Potential. *Adv. Energy Mater.* **2020,** *10* (13), 1903109.

(41) Mosconi, E.; Meggiolaro, D.; Snaith, H. J.; Stranks, S. D.; De Angelis, F. Light-Induced Annihilation of Frenkel Defects in Organo-Lead Halide Perovskites. *Energy Environ. Sci.* **2016,** *9* (10), 3180-3187.

(42) deQuilettes, D. W.; Zhang, W.; Burlakov, V. M.; Graham, D. J.; Leijtens, T.; Osherov, A.; Bulović, V.; Snaith, H. J.; Ginger, D. S.; Stranks, S. D. Photo-Induced Halide Redistribution in Organic–Inorganic Perovskite Films. *Nat. Commun.* **2016,** *7* (1), 11683.

(43) Kim, J.; Godin, R.; Dimitrov, S. D.; Du, T.; Bryant, D.; McLachlan, M. A.; Durrant, J. R. Excitation Density Dependent Photoluminescence Quenching and Charge Transfer Efficiencies in Hybrid Perovskite/Organic Semiconductor Bilayers. *Adv. Energy Mater.* **2018,** *8* (35), 1802474.

(44) Lin, Y.; Shen, L.; Dai, J.; Deng, Y.; Wu, Y.; Bai, Y.; Zheng, X.; Wang, J.; Fang, Y.; Wei, H.; Ma, W.; Zeng, X. C.; Zhan, X.; Huang, J. Π-Conjugated Lewis Base: Efficient Trap-Passivation and Charge-Extraction for Hybrid Perovskite Solar Cells. *Adv. Mater.* **2017,** *29* (7), 1604545.

(45) Zhang, J.; Bai, D.; Jin, Z.; Bian, H.; Wang, K.; Sun, J.; Wang, Q.; Liu, S. 3d–2d–0d Interface Profiling for Record Efficiency All-Inorganic $Cspbbri_2$ Perovskite Solar Cells with Superior Stability. *Adv. Energy Mater.* **2018,** *8* (15), 1703246.

(46) Tan, H.; Jain, A.; Voznyy, O.; Lan, X.; García de Arquer, F. P.; Fan, J. Z.; Quintero-

Bermudez, R.; Yuan, M.; Zhang, B.; Zhao, Y.; Fan, F.; Li, P.; Quan, L. N.; Zhao, Y.; Lu, Z.-H.; Yang, Z.; Hoogland, S.; Sargent, E. H. Efficient and Stable Solution-Processed Planar Perovskite Solar Cells Via Contact Passivation. *Science* **2017,** *355* (6326), 722-726.

(47) Xing, G.; Mathews, N.; Sun, S.; Lim, S. S.; Lam, Y. M.; Grätzel, M.; Mhaisalkar, S.; Sum, T. C. Long-Range Balanced Electron- and Hole-Transport Lengths in Organic-Inorganic $CH_3NH_3PbI_3$. *Science* **2013,** *342* (6156), 344-347.

(48) Juarez-Perez, E. J.; Ono, L. K.; Maeda, M.; Jiang, Y.; Hawash, Z.; Qi, Y. Photodecomposition and Thermal Decomposition in Methylammonium Halide Lead Perovskites and Inferred Design Principles to Increase Photovoltaic Device Stability. *J. Mater. Chem. A* **2018,** *6* (20), 9604-9612.

(49) Motti, S. G.; Meggiolaro, D.; Barker, A. J.; Mosconi, E.; Perini, C. A. R.; Ball, J. M.; Gandini, M.; Kim, M.; De Angelis, F.; Petrozza, A. Controlling Competing Photochemical Reactions Stabilizes Perovskite Solar Cells. *Nat. Photonics* **2019,** *13* (8), 532-539.

(50) Kerner, R. A.; Xu, Z.; Larson, B. W.; Rand, B. P. The Role of Halide Oxidation in Perovskite Halide Phase Separation. *Joule* **2021,** *5* (9), 2273-2295.

(51) Endres, J.; Egger, D. A.; Kulbak, M.; Kerner, R. A.; Zhao, L.; Silver, S. H.; Hodes, G.; Rand, B. P.; Cahen, D.; Kronik, L.; Kahn, A. Valence and Conduction Band Densities of States of Metal Halide Perovskites: A Combined Experimental–Theoretical Study. *J. Phys. Chem. Lett.* **2016,** *7* (14), 2722-2729.

(52) Schubert, S.; Klumbies, H.; Müller-Meskamp, L.; Leo, K. Electrical Calcium Test for Moisture Barrier Evaluation for Organic Devices. *Rev. Sci. Instrum.* **2011,** *82* (9), 094101.

(53) Abate, A.; Leijtens, T.; Pathak, S.; Teuscher, J.; Avolio, R.; Errico, M. E.; Kirkpatrik, J.; Ball, J. M.; Docampo, P.; McPherson, I.; Snaith, H. J. Lithium Salts as "Redox Active" P-Type Dopants for Organic Semiconductors and Their Impact in Solid-State Dye-Sensitized Solar Cells. *Phys. Chem. Chem. Phys.* **2013,** *15* (7), 2572-2579.

(54) Kong, J.; Shin, Y.; Röhr, J. A.; Wang, H.; Meng, J.; Wu, Y.; Katzenberg, A.; Kim, G.;

Kim, D. Y.; Li, T.-D.; Chau, E.; Antonio, F.; Siboonruang, T.; Kwon, S.; Lee, K.; Kim, J. R.; Modestino, M. A.; Wang, H.; Taylor, A. D. Co_2 Doping of Organic Interlayers for Perovskite Solar Cells. *Nature* **2021,** *594* (7861), 51-56.

(55) Erdélyi, M. Halogen Bonding in Solution. *Chem. Soc. Rev.* **2012,** *41* (9), 3547-3557.

(56) Yang, X.; Ni, Y.; Zhang, Y.; Wang, Y.; Yang, W.; Luo, D.; Tu, Y.; Gong, Q.; Yu, H.; Zhu, R. Multiple-Defect Management for Efficient Perovskite Photovoltaics. *ACS Energy Lett.* **2021,** *6* (7), 2404-2412.

(57) Ruth, A.; Brennan, M. C.; Draguta, S.; Morozov, Y. V.; Zhukovskyi, M.; Janko, B.; Zapol, P.; Kuno, M. Vacancy-Mediated Anion Photosegregation Kinetics in Mixed Halide Hybrid Perovskites: Coupled Kinetic Monte Carlo and Optical Measurements. *ACS Energy Lett.* **2018,** *3* (10), 2321-2328.

(58) Muscarella, L. A.; Ehrler, B. The Influence of Strain on Phase Stability in Mixed-Halide Perovskites. *Joule* **2022,** *6* (9), 2016-2031.

(59) Knight, A. J.; Patel, J. B.; Snaith, H. J.; Johnston, M. B.; Herz, L. M. Trap States, Electric Fields, and Phase Segregation in Mixed-Halide Perovskite Photovoltaic Devices. *Adv. Energy Mater.* **2020,** *10* (9), 1903488.

(60) Kim, G. Y.; Senocrate, A.; Wang, Y.-R.; Moia, D.; Maier, J. Photo-Effect on Ion Transport in Mixed Cation and Halide Perovskites and Implications for Photo-Demixing. *Angew. Chem. Int. Ed.* **2021,** *60* (2), 820-826.

(61) Wang, Y.-R.; Kim, G. Y.; Kotomin, E.; Moia, D.; Maier, J. Photo De-Mixing in Mixed Halide Perovskites: The Roles of Ions and Electrons. *J. Phys. Energy* **2022,** *4* (1), 011001.

(62) Brennan, M. C.; Toso, S.; Pavlovetc, I. M.; Zhukovskyi, M.; Marras, S.; Kuno, M.; Manna, L.; Baranov, D. Superlattices Are Greener on the Other Side: How Light Transforms Self-Assembled Mixed Halide Perovskite Nanocrystals. *ACS Energy Lett.* **2020,** *5* (5), 1465-1473.

(63) Zhang, H.; Fu, X.; Tang, Y.; Wang, H.; Zhang, C.; Yu, W. W.; Wang, X.; Zhang, Y.; Xiao, M. Phase Segregation Due to Ion Migration in All-Inorganic Mixed-Halide Perovskite Nanocrystals. *Nat. Commun.* **2019,** *10* (1), 1088.

(64) Mathew, P. S.; Samu, G. F.; Janáky, C.; Kamat, P. V. Iodine (I) Expulsion at Photoirradiated Mixed Halide Perovskite Interface. Should I Stay or Should I Go? *ACS Energy Lett.* **2020,** *5* (6), 1872-1880.

(65) Troian-Gautier, L.; Turlington, M. D.; Wehlin, S. A. M.; Maurer, A. B.; Brady, M. D.; Swords, W. B.; Meyer, G. J. Halide Photoredox Chemistry. *Chem. Rev.* **2019,** *119* (7), 4628-4683.

(66) Al-Ashouri, A.; Magomedov, A.; Roß, M.; Jošt, M.; Talaikis, M.; Chistiakova, G.; Bertram, T.; Márquez, J. A.; Köhnen, E.; Kasparavičius, E.; Levcenco, S.; Gil-Escrig, L.; Hages, C. J.; Schlatmann, R.; Rech, B.; Malinauskas, T.; Unold, T.; Kaufmann, C. A.; Korte, L.; Niaura, G.; Getautis, V.; Albrecht, S. Conformal Monolayer Contacts with Lossless Interfaces for Perovskite Single Junction and Monolithic Tandem Solar Cells. *Energy Environ. Sci.* **2019,** *12* (11), 3356-3369.

(67) Hoffman, J. B.; Astridge, D. D.; Park, S. Y.; Zhang, F.; Yang, M.; Moore, D. T.; Harvey, S. P.; Zhu, K.; Sellinger, A. Polymer Hole Transport Material Functional Group Tuning for Improved Perovskite Solar Cell Performance. *ACS Appl. Energy Mater.* **2022,** *5* (7), 8601-8610.

TOC Graphic